Design and Performance Analysis of Superconducting Rim-Driven Synchronous Motors for Marine Propulsion

Amir Hassannia and Ahmad Darabi

***Abstract*—Rim-driven thrusters have received much attention concerning the potential benefits in vibration and hydrodynamic characteristics, which are of great importance in marine transportation systems. In this sense, the rim-driven permanent magnet, brushless dc, and induction motors have been recently suggested to be employed as marine propulsion motors. On the other hand, high-temperature superconducting (HTS) synchronous motors are becoming much fascinating, particularly in transport applications, regarding some considerable advantages such as low loss, high efficiency, and compactness. However, the HTS-type rim-driven synchronous motor has not been studied yet. Therefore, this paper is devoted to a design practice of rim-driven synchronous motors with HTS field winding. A detailed design procedure is developed for the HTS rim-driven motors, and the design algorithm is validated applying the finite element (FE) method. The FE model of a three-phase 2.5-MW HTS rim-driven synchronous motor is utilized, and the electromagnetic characteristics of the motor are then evaluated. The goal is to design an HTS machine fitted in a thin duct to minimize the hydrodynamic drag force. The design problem exhibits some difficulties while considering various constraints.**

***Index Terms*—Design, finite elements, marine propulsion, rim–driven synchronous motor, superconductor.**

I. Introduction

ELECTRIC propulsion systems are widely used in marine transportation as well as land and air transportation and other industrial applications [1]. Many advantages of electrical propulsion extend their application in warship and military submarine vessels [2], [3]. The azimuth, podded, and rim-driven thrusters are three important types of maritime electric propulsion system. The rim-driven thruster is distinguished from other thrusters because of its benefits in hydrodynamic performance, mechanical noise, hydraulic power dissipation, natural lubrication, etc. [1], [4]–[7].

Although many advantages, some problems are involved in rim-driven motor design. The propeller imposes special constraints on propulsion motor [7]. The nominal power, speed, and inner diameter of the rotor are given by the rated power, speed, and outer diameter of the propeller, respectively [8]. The motor radial thickness (stator outer radius minus rotor inner radius) is the next limitation. This dimension forms the surface that is directly in contact with the water flow and should be compacted as much as possible to reduce the hydrodynamic drag force [9]. The axial length of the machine is also limited by the duct length, which can be 1.5 times larger than the propeller length [8]. Furthermore, the water flow between the rotor and the stator imposes a relatively large air gap, which affects the motor magnetic design [8].

The rim-driven propeller concept has been known for a long time, but the marine rim-driven motors came into wide use in recent years. The permanent magnet (PM), brushless dc (BLDC), and induction motors are well known in marine rim-driven thruster. In 2004, a 100-kW PM rim-driven motor was designed and built [10]. Sometime later, a new algorithm was developed to design a BLDC rim-driven propulsion motor in 2006 [11]. These activities were followed by designing a 183-kW induction rim-driven motor in 2010 [12]. The performance analysis demonstrates a minor decay in operation characteristics of the rim-driven induction motor, as compared to a similar typical induction motor [12]. Recently, the axial flux PM motor has also been considered in rim-driven thrusters [13].

Superconducting motors are an attractive option in marine propulsion due to their potential benefits such as high power density, light weight, low loss, and high efficiency. Design knowledge and technology of high-temperature superconducting (HTS) propulsion motors has been developed greatly through designing and building various types of HTS motors for azimuth and podded thrusters [14]–[16]. Nevertheless, the superconducting rim-driven propulsion motor seems to be a novel case. In this paper, a new structure of HTS rim-driven motor is presented to embed the benefits of HTS motor in a rim-driven marine propulsion system. Various design considerations are taken into account to plan an HTS motor that satisfies the rim-driven propulsion system requirements.

The mentioned limitations for rim-driven thruster arise particularly in the HTS propulsion motor. Radial thickness of superconducting motors is generally large due to rather large air gap. Therefore, it is somewhat difficult to design an enough thin HTS motor for a rim-driven thruster.

The groundwork of the present paper is a 2.5-MW PM rim-driven motor, which has been recently designed [8]. A small-size prototype (100 kW) of a similar motor has been

Manuscript received March 9, 2013; revised June 16, 2013 and July 22, 2013; accepted August 14, 2013. Date of current version September 23, 2013. This paper was recommended by Associate Editor M. Parizh.

The authors are with the Faculty of Electrical and Robotic Engineering, University of Shahrood, Shahrood 36199 95161, Iran (e-mail: amir.hassannia@gmail.com; darabi_ahmad@hotmail.com).

Color versions of one or more of the figures in this paper are available online at http://ieeexplore.ieee.org.

Digital Object Identifier 10.1109/TASC.2013.2280346

TABLE I
DESIGN PARAMETERS OF HTS RIM-DRIVEN MOTOR

Parameters	Value	Unit
Rated power	2.5	MW
Effective line voltage	400	V
Frequency	55	Hz
Rated speed	220	rpm
Rotor inner diameter	3000	mm
Maximum axial length	600	mm
Maximum radial thickness	165	mm

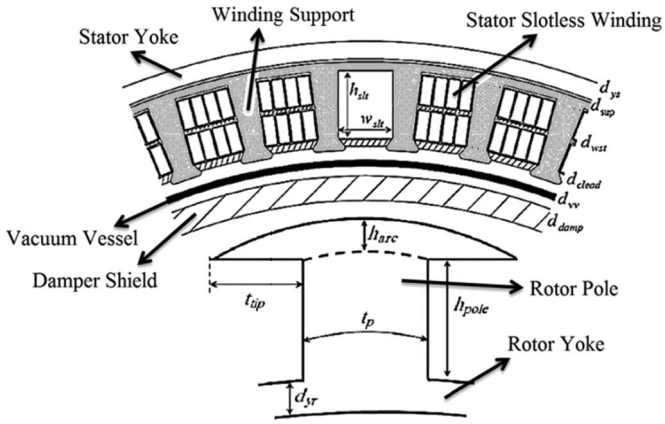

Fig. 1. Overview of selected structure.

manufactured. The given test results of this motor validates the design algorithm of PM rim-driven motor [10]. The rated values, required features, and constraints of 2.5-MW PM rim-driven machine are given in Table I. Besides the design algorithm, the second goal of the present paper is to design an HTS rim-driven motor with the constraints and rated values similar to the existing PM-type motor to be able to compare characteristics of both motors in the end.

Salient-pole radial-flux synchronous structure with HTS excitation coils in rotor is picked for the HTS rim-driven motor. A total of 30 poles is needed to provide the rated speed at nominal frequency. The concept of the selected structure is shown in Fig. 1. This is the conventional structure of a synchronous machine, which is optimized for rim-driven superconducting operation.

II. BASIC PARAMETERS AND DESIGN ALGORITHM

The first stage is selecting the working temperature of HTS coils (t_w), which affects significantly the field current density and consequently size of the machine. Critical current of field winding is increased by any decrement in HTS working temperature. As a result, the volume of field winding and consequently size of the machine can be reduced. Nevertheless, this issue imposes the need of a stronger and larger cooling system. A reasonable tradeoff between these issues usually yields to rather high working temperature in HTS propulsion motors [8], [15], [17]. The parameter is typically selected as $t_w = 75$ K in this work.

The air-gap flux density (B_{ag}) and electrical loading (ac) are the most effective parameters in machine size. The machine core magnetic saturation is the key criterion to choose the maximum air-gap flux density in conventional machines. This parameter is selected fairly high to reduce the weight and volume of the machine. The HTS coils can provide high magnetic flux density, which is the main reason of superconducting machines' compactness. However, many simulations show that besides decreasing the volume and axial length of the machine, the radial thickness is increased by any increment in the air-gap flux density. Therefore, the superconducting rim-driven motor design problem involves an exceptional tradeoff between compactness and radial thickness minimization.

One of the most critical matters is assigning a proper value for the electrical loading defined as

$$ac = \frac{Z \cdot I_{con}}{\pi \cdot D_{is}} \tag{1}$$

in which Z is total number of conductors of stator winding, I_{con} is the current of each conductor, and D_{is} is inner diameter of the stator. Relatively low voltage necessitates employing parallel coils in the stator winding. The number of turns of the winding in series is related to the number of slots per pole per phase proportionally. Therefore, the electrical loading factor can be chosen among some individual values within a typical range $(ac_l < ac < ac_u)$.

Commonly both ac and B_{ag} have the most significant influences on the total size of the machine so that larger values of them yield to a smaller size machine. Similar to B_{ag}, the simulations show that sometime any increase in electrical loading increases radial thickness of the HTS machine beside the volume and axial length of the machine decrease. This can be related to the existing complications in rim-driven HTS motor structure, compelling some caution when assigning values to B_{ag} and ac, particularly when the purpose is to obtain a thin and compact machine. In this sense, the algorithm, as shown in Fig. 2, starts with relatively a low value of B_{ag}, and then, its value is increased gradually until the value of axial length becomes less than the maximum predefined value. For each value of B_{ag}, the value of ac is adjusted nearly to the maximum value (ac_u) so that the number of winding turns deduced from (1) becomes an integer coefficient of the number of slots per pole per phase. It is done easily by an internal loop. Final values of the air-gap flux density and electrical loading factor obtained by this algorithm for the case study machine of the present paper are $B_{ag} = 0.65$ T and $ac = 43883$ A/m.

Rotor, stator, and air gap are the main parts of the machine in design procedure. A number of considerations are needed to properly design of these parts to realize the desired thin and compact machine.

III. AIR GAP DESIGN

The vacuum vessel is an isolation layer between cold rotor and warm stator that occupies about 4 mm of radial thickness typically [18], [19]. Damper shield thickness is designed as an appropriate percentage of magnetic penetration depth (δ_{thk}). The problem is to choose a thick and effective damper shield or a thin and less effective one. In this case, the damper shield is designed as thin as possible via a tradeoff. The parameter is

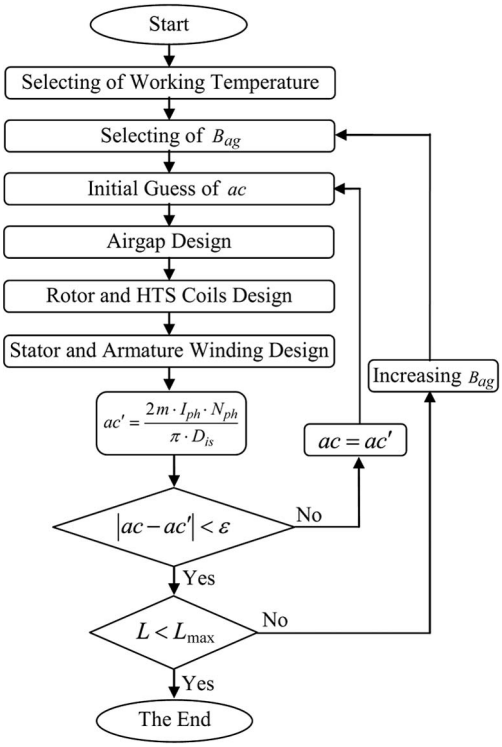

Fig. 2. General design process.

considered as 80% of magnetic penetration depth according to the following equation [20]:

$$d_{damp} = 0.8 \times \delta_{thk} = \frac{0.8}{\sqrt{\pi \mu f \sigma K_T}} \tag{2}$$

where μ is magnetic permeability, σ is electric conductivity at room temperature, and f is stator frequency. Parameter K_T represents the thermal correction factor that is calculated as [8]

$$K_T = \frac{234 + t_0}{234 + t_w} \tag{3}$$

where $t_0 = 293$ K is room temperature. The stator teeth magnetic saturation is a major limitation in usual synchronous machine. Therefore, the slotless stator is more popular in HTS machine due to strong air-gap magnetic field, which is provided by the superconducting field winding [21]. The slotless stator reduces the winding layer thickness and consequently the total radial thickness of the motor. The stator winding layer depth (d_{wst}) can be calculated as

$$d_{wst} = \frac{ac}{J \cdot k_{full} \cdot k_{iso} \cdot k_{\sup}} \tag{4}$$

where J is the stator winding current density; k_{full} is the stator winding fullness factor; k_{iso} and $k_{\sup}$ are defined to consider the winding isolation and winding support, respectively.

IV. Rotor Design

The rotor consists of rotor yoke, rotor poles, and HTS coils. The pole pitch angle is calculated considering the total 15 pairs of poles. The ratio of pole body angle (θ_{tp}) to pole pitch angle (θ_p) is a key parameter that affects the pole body saturation, rotor leakage flux, air-gap flux harmonic content, available space for HTS field winding, and notably radial thickness of the machine. That is

$$K_p = \frac{\theta_{tp}}{\theta_p}. \tag{5}$$

Obviously, parameter K_p has to be increased by the air-gap flux density increment proportionally to prevent the pole body saturation. The algorithm offers the value of 0.4225 for K_p by a tradeoff between field winding space and machine radial thickness.

The arc length of rotor body (t_p) and the rotor yoke thickness (d_{yr}) are found after a number of loops and corrections through following equations:

$$t_p = \theta_{tp}(R_{ir} + d_{yr}) \tag{6}$$

$$d_{yr} = 0.34 \times t_p \tag{7}$$

where R_{ir} is inner rotor radius. The pole height (h_{pole}) is calculated using a similar iteration. The procedure starts with an initial guess of pole height. The average flux density of pole body (B_{tp}) is calculated as

$$B_{tp} = \frac{2}{\pi} B_{ag} \left(\frac{\theta_p \cdot R_{is}}{t_p(1 - k_{leak})} \right) \tag{8}$$

where $R_{is} = R_{ir} + d_{yr} + h_{pole} + Ag$ is inner radius of stator yoke, and Ag is total air gap. Parameter k_{leak} represents the leakage flux factor, which was defined as

$$k_{leak} = 1 - \frac{\varphi_{st}}{\varphi_r} \approx 0.03 \tag{9}$$

where φ_{st} and φ_r are maximum flux in stator and rotor yoke, respectively. The leakage flux factor of the case study machine was found after some loops and corrections as 3%. The required magnetomotive force per pole can be obtained considering the air gap reluctance $(\Re_{ag})$ and desired flux in rotor body (φ_{tp}). That is

$$\begin{aligned} N_f I_f &= (1 - k_{leak}) \cdot \varphi_{tp} \cdot \Re_{ag} \\ &= \frac{(1 - k_{leak}) \cdot B_{tp} \cdot t_p \cdot Ag}{\mu_0 \left(\frac{\theta_p + \theta_{tp}}{2} \right) \left(R_{is} - \frac{Ag}{2} \right)}. \end{aligned} \tag{10}$$

Rated field current depends on HTS wire model, working temperature, and magnetic flux density on HTS coils. The Superpower-SCS3050 wire is selected for the case study HTS motor. The wire specifications are shown in Table II [22]. Fig. 3 shows the constitutive layers of HTS wire, in which the thickness of all layers is approximately 0.1 mm. Total thickness of the wire considering the isolation layer is about 0.2 mm [22].

According to Table II, Maximum allowable current value of superconducting wire is 75 A at 77 K and zero magnetic field. Working temperature of rotor is assumed 75 K to secure assumption of critical current equal to $I_c = 75$ A in zero magnetic field. Critical current of HTS wire varies by normal flux density, as shown in Fig. 4 [23]. If the permitted maximum value of normal component of flux density is assumed 0.6 T, according to the specification of HTS wire, the critical current

TABLE II
SPECIFICATIONS OF SUPERCONDUCTING TAPE

Parameters	Value	Unit
Critical current (at 77 K)	75	A
Width	3	mm
Thickness	0.1	mm
Critical tensile stress	> 550	MPa
Critical axial tensile strain	45	%
Critical bend diameter	11	mm

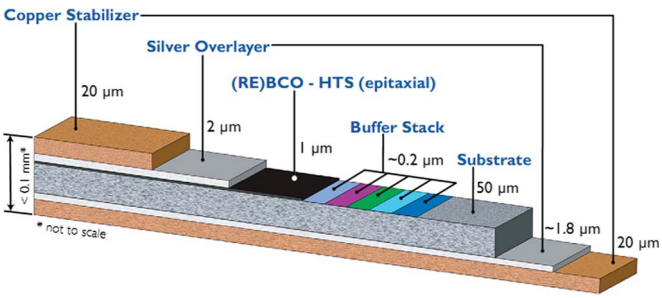

Fig. 3. Structure of HTS tape (without electrical isolator) [22].

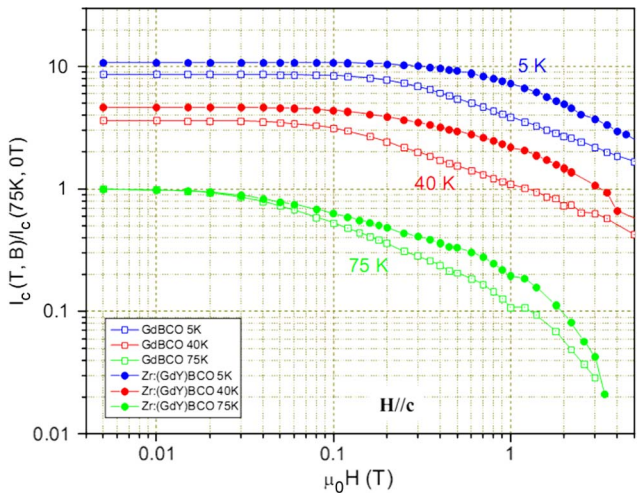

Fig. 4. Critical current of HTS tape as a function of magnetic field at different working temperature [23].

of superconducting coils will be 23 A. Therefore, the rated value of the field current has to be by a safety margin less than 23 A, e.g., $I_f = 18$ A. Taking this value for the field current and evaluating the ampere turns per pole using (10), the number of turns of field winding per pole is simply calculated.

The HTS coil was used in pancake structure for winding convenience. Considering the HTS wire dimensions, the width of each pancake is an integer coefficient of 0.2 mm and the pancake height is 3 mm. Due to limited available space between rotor poles and consequently limited pancake width, several series pancakes are needed to beget the required turns of field winding. Therefore, the pole height will increase in an iterative loop to provide enough space for pancakes. After a few number of iteration, 1153 turns of field coil per pole formed in four pancakes, as shown in Fig. 5. The pancake formation was

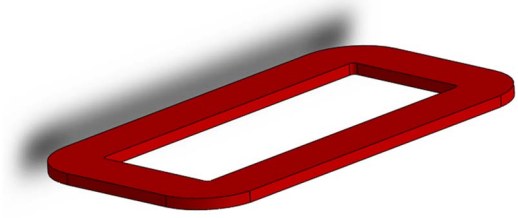

Fig. 5. HTS excitation coil.

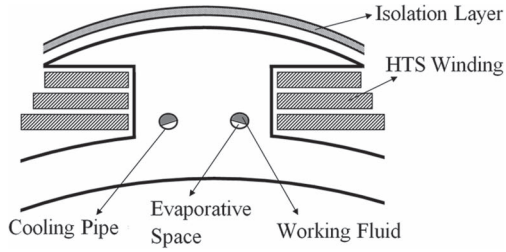

Fig. 6. Sketch of PEC system.

performed considering the critical bend diameter of SCS-3050 HTS wire.

V. COOLING SYSTEM

Design of the cooling system is a voluminous work, which is outside the scope of this paper, but it is necessary to consider the main requirements of cooling system. The thermosyphon, open evaporative cooling, and piping evaporative cooling (PEC) are three customary refrigeration approaches in superconducting machines [24], where the PEC is more conventional for large-size and low-speed machine [24]. The system consists of cool isolated rotor with embedded cooling pipe in rotor core according to Fig. 6. An enough space is considered for cooling pipe in the studied motor.

VI. STATOR DESIGN

Due to relatively low rated voltage, 15 parallel circuits are considered in the stator winding. The number of stator winding turns in series (N_{ph}) is calculated as

$$N_{ph} = \frac{\pi \cdot D_{is} \cdot ac}{2m \cdot I_{ph}} \tag{11}$$

where m is the number of phases, and I_{ph} is rated phase current. Parameter N_{ph} is an integer coefficient of number of co-slot per pole per phase. The authorized value of ac realizes the correct value of N_{ph}.

VII. AXIAL LENGTH

The axial length of machine is determined by the required flux per rotor pole. This quantity is a function of chosen induced voltage in armature. The terminal rated voltage is a common choice for armature-induced voltage in conventional synchronous motors. Lagging power factor is a result of this choice. In this situation, armature reaction can increases the core flux density of machine. On the other hand, rim-driven

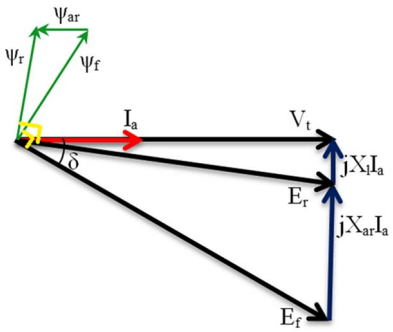

Fig. 7. Phasor diagram of the machine.

motors are usually designed very near to the magnetic saturation point to reduce the radial thickness. Therefore, lagging-power-factor rim-driven synchronous motor may be saturated magnetically by armature reaction. After a number of loops and corrections, the armature-induced voltage is selected as 1.027 times larger than terminal voltage to achieve the unity power factor motor. Phasor diagram of machine is shown in Fig. 7. The unity power factor machine will not saturate in partial loading condition. The axial length of the machine can be calculated by following equations:

$$E_f = 1.027 \times V_t \tag{12}$$

$$\varphi_p = \frac{E_f}{4.44f \cdot N_{ph} \cdot k_w} \tag{13}$$

$$L = \frac{\varphi_p}{(1 - k_{leak})\, t_p \cdot B_{tp}} \tag{14}$$

where E_f and V_t are the armature-induced and terminal voltages, respectively, φ_p is flux per pole, and k_w is winding factor.

As mentioned earlier, there is a constraint on axial length of rim-driven propulsion motor. If it exceeds the predefined maximum value, the design algorithm of Fig. 2 needs to be repeated with a higher air-gap flux density until all constraints including axial length requirement be satisfied. However, if the design algorithm is applied to design the HTS rim-driven motor with the same specifications of the PM motor given in Table I, the main design parameters of the studied HTS motor will be as briefly listed in Table III.

VIII. FE Analysis

Finite element (FE) analysis is performed to evaluate the design algorithm accuracy and investigation of main performance characteristics. The flux density in different parts of machine was calculated during design procedure. These results are verified by developing a 2-D FE model of machine. Fig. 8 shows the flux density distribution for a pair of poles in no-load condition. The figure shows that the flux density in rotor core, stator core, and air gap is matched to that calculated in design procedure.

Furthermore, the maximum flux density of 0.577 T occurs on the corner of HTS coil, as shown in Fig. 9. The permitted value of this parameter has been assumed 0.6 T in design procedure, which guarantees the valid performance of HTS

TABLE III
KEY DESIGN PARAMETERS

Parameters	Value	Unit
Electrical loading	43883	A/m
Air gap flux density	0.65	T
Rotor yoke thickness	48	mm
Stator yoke thickness	48	mm
Rotor pole height	12	mm
Total air gap width	38.5	mm
Stator outer Radius	1650.5	mm
Total machine thickness	150.5	mm
Machine core axial length	363	mm
Turns of field winding	1153	
Turns of stator winding in series	20	

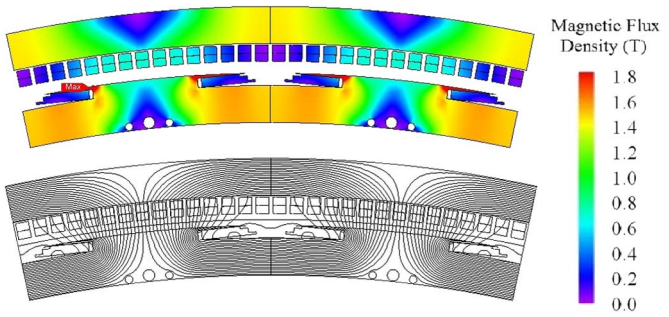

Fig. 8. No-load flux density distribution.

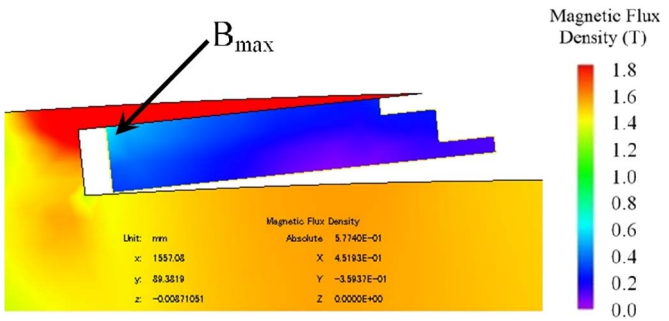

Fig. 9. Flux density distribution on excitation coil.

coil. The leakage flux factor is another parameter, which can be calculated and verified from FE model as follows:

$$k_{leak} = 1 - \frac{\varphi_{st}}{\varphi_r} = 1 - \frac{0.0248}{0.0255} = 0.0274. \tag{15}$$

The armature-induced voltage is shown in Fig. 10, which is obtained via FE model by rotor step rotation with rated speed and nominal field current. The voltages include rather noticeable third harmonic component, which is removed in current wave form due to nongrounded star connection of stator winding.

A similar model was developed to evaluate the motor performance in under-load condition. The FE model is coupled with a current source drive model. The supply source applies three-phase rated current wave to the stator winding. By a loop and correction trial, the phase difference of armature-induced

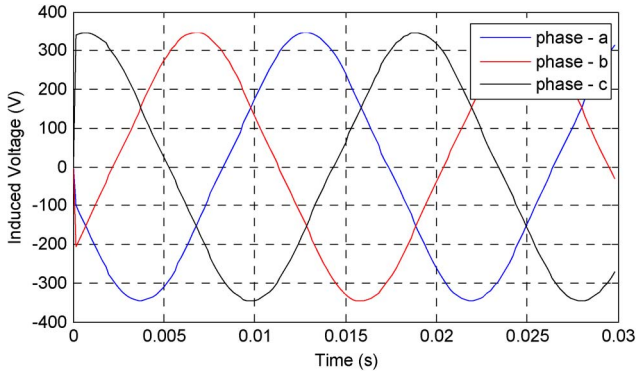

Fig. 10. Armature-induced voltage.

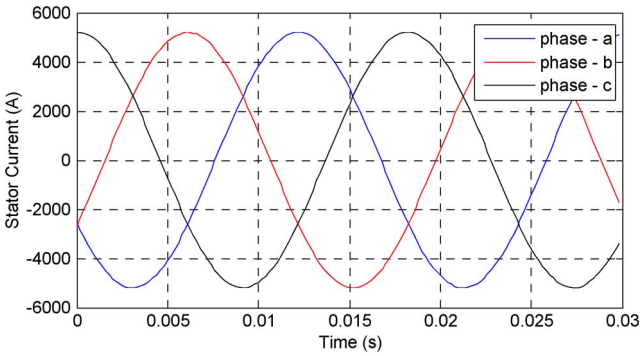

Fig. 11. Three-phase current applied to the armature by drive system.

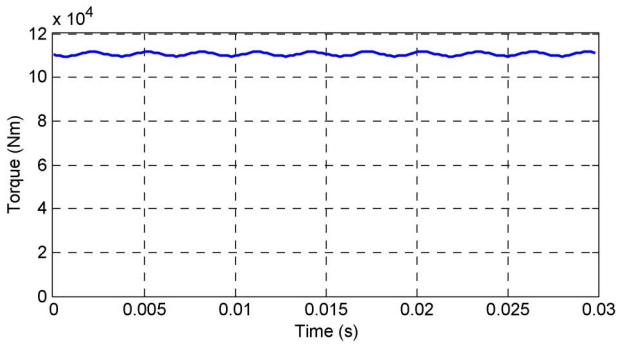

Fig. 12. Rotor-induced torque.

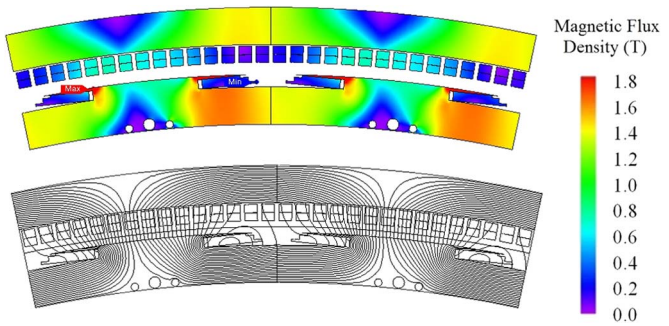

Fig. 13. Full-load flux density distribution.

TABLE IV
KEY PERFORMANCE CHARACTERISTICS OF THE MACHINE

Parameters	Value	Unit
Rotor yoke flux density	1.48	T
Stator yoke flux density	1.44	T
Winding joule loss	26008	W
Core loss	17197	W
Machine total losses	43205	W
Efficiency (Core and Joule loss only)	98.3	%
Power factor	1	-

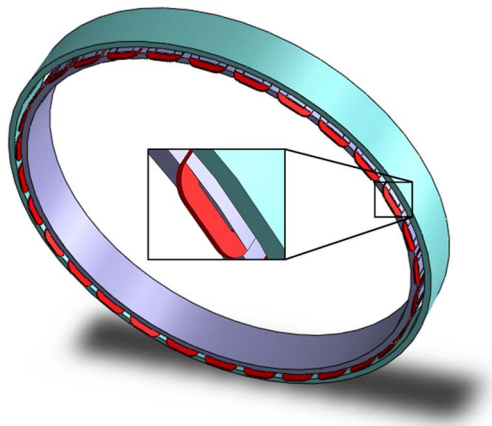

Fig. 14. Three-dimensional view of the machine core and excitation coils.

voltage and terminal voltage is determined as $\delta = 0.227$ rad to achieve the rated torque. The phase of stator current is equal to phase of terminal voltage. The stator currents and rotor-induced torque are shown in Figs. 11 and 12, respectively.

In the unity power factor motor, the armature reaction (ψ_{ar}) reduces the absolute value of rotor magnetic field (ψ_f), as shown in Fig. 7. The flux density distribution in under-load condition verifies the flux reduction prediction, as shown in Fig. 13. Furthermore, the flux density distribution is somewhat asymmetric due to phase shifting of its phasor according to Fig. 7.

The winding and core losses and consequently the electromagnetic efficiency of the motor are obtained from FE model in rated power condition. Some important performance characteristics that were obtained from the FE model are shown in Table IV. A 3-D view of stator and rotor core together with HTS coils is shown in Fig. 14.

Overall, dimensions and electromagnetic efficiency of HTS rim-driven motor and those of PM rim-driven motor are given in Table V for comparison. As expected and seen from this table, the HTS motor is fairly thin and compact, while the electromagnetic losses is smaller and efficiency is higher comparing with PM motor. All these can be considered as the advantages and superiors of the rim-driven HTS motor. Furthermore, since the radial thickness of HTS motor is somewhat smaller, the undesired drag force would be fewer, which has not been considered in this paper.

IX. CONCLUSION

In this paper, the concept and a proper structure of the superconducting rim-driven motor were investigated, and associated design algorithm was developed to provide the certain design requirements of the new machine. A rim-driven

TABLE V
COMPARISON OF PM AND HTS MOTORS

Parameters	PM Motor	HTS Motor
Rated power (MW)	2.5	2.5
Rated voltage (V)	400	400
Rated speed (rpm)	220	220
Electromagnetic efficiency (%)	96	98.3
Radial thickness (mm)	165	150.5
Axial length (considering the end winding) (mm)	600	505

superconducting motor was designed for the purpose to be employed as electric propulsion of a relatively medium size submarine. The design algorithm of machine was validated by 2-D FE modeling. It has been discussed that the diameter of ordinary HTS motors, which is commonly large comparing with axial length, can be reduced significantly by tuning some key design parameters of a rim-driven-type superconducting motor. The undesired drag force can be decreased significantly in resultant thin motor. These form the proposed structure as an eligible electric propulsion system owning superior and advantages of both rim-driven and superconducting motor.

ACKNOWLEDGMENT

The authors would like to thank the Research Center for Marine Propulsions, University of Shahrood, and the Marine Industry Organization for the support and information.

REFERENCES

[1] J. F. Gieras, *Advancements in Electric Machines*. Rockford, IL, USA.: Springer, 2008.
[2] D. S. Parker and C. G. Hodge, "The electric warship," in *Proc. 8th Int. Conf. Elect. Mach. Drives*, 1997, pp. 319–325.
[3] J. K. Holt, "Propulsion systems for submarine vessels," U.S. Patent 5 306 183, Apr. 26, 1994.
[4] M. F. Hsieh, J. H. Chen, Y. H. Yeh, C. L. Lee, P. H. Chen, Y. C. Hsu, and Y. H. Chen, "Integrated design and realization of a hubless rim-driven thruster," in *Proc. IEEE 33rd Annu. Conf. IECON*, Taipei, Taiwan, 2007, pp. 3033–3038.
[5] A. Y. Yakovlev, M. A. Sokolov, and N. V. Marinich, "Numerical design and experimental verification of a rim-driven thruster," presented at the 2nd Int. Symp. Marine Propulsors, Hamburg, Germany, 2011.
[6] K. H. Kim, S. Turnock, J. Ando, P. Becchi, E. Korkut, A. Minchev, E. Y. Semionicheva, S. H. Van, and W. X. Zhou, "The propulsion committee: Final report and recommendations to the 25th ITTC," in *Proc. Int. Towing Tank Conf.*, Fukuoka, Japan, 2008, pp. 115–121.
[7] C. Pashias and S. R. Turnock, Hydrodynamic design of bi-directional, rim-driven ducted thruster suitable for underwater vehicles, Univ. Southampton, Southampton, U.K. [Online]. Available: http://eprints.soton.ac.uk/id/eprint/46052
[8] Q. Krovel, "Design of large permanent magnetized synchronous electric machines," Ph.D. dissertation, Dept. Elect. Pow. Eng., Norwegian Univ. Sci. Tech., Trodheim, Norway, 2011.
[9] S. M. Sharkh and S. H. Lai, "Slotless PM brushless motor with helical edge-wound laminations," *IEEE Trans. Energy Conv.*, vol. 24, no. 3, pp. 594–598, Sep. 2009.
[10] O. Krovel, R. Nilssen, S. E. Skaar, E. Lvli, and N. Sandoy, "Design of an integrated 100 kW permanent magnet synchronous machine in a prototype thruster for ship propulsion," in *Proc. ICEM*, Cracow, Poland, 2004, pp. 117–123.
[11] S. H. Lai, "Design optimisation of a slotless brushless permanent magnet DC motor with helically-wound laminations for underwater rim-driven thrusters," Ph.D. dissertation, Facul. Eng. Sci. Math., Univ. Southampton, Southampton, U.K., 2006.
[12] P. M. Tuohy, A. C. Smith, and M. Husband, "Induction rim-drive for a marine propulsor," presented at the 5th IET Int. Conf. Power Electron., Machines Drives, Brighton, U.K., 2010.
[13] S. Djebarri, J. F. Charpentier, F. Scuiller, M. Benbouzid, and S. Guemard, "Rough design of a double-stator axial flux permanent magnet generator for a rim-driven marine current turbine," in *Proc. IEEE ISIE*, 2012, pp. 1450–1455.
[14] B. Gamble, G. Snitchler, and T. MacDonald, "Full power test of a 36.5 MW HTS propulsion motor," *IEEE Trans. Appl. Supercond.*, vol. 21, no. 3, pp. 1083–1088, Jun. 2011.
[15] J. Li and K. T. Chau, "A novel HTS PM vernier motor for direct-drive propulsion," *IEEE Trans. Appl. Supercond.*, vol. 21, no. 3, pp. 1175–1179, Jun. 2011.
[16] D. Sugyo, Y. Kimura, T. Sano, K. Yamaguchi, K. Tsuzuki, R. Taguchi, M. Izumi, M. Miki, M. Kitano, H. Sugimoto, and H. Fujimoto, "Bi-2223 field-poles without iron core for an axial type of HTS propulsion motor," *IEEE Trans. Appl. Supercond.*, vol. 19, no. 3, pp. 1687–1691, Jun. 2009.
[17] Y. Kim, T. Ki, H. Kim, S. Jeong, J. Kim, and J. Jung, "High temperature superconducting motor cooled by on-board cryocooler," *IEEE Trans. Appl. Supercond.*, vol. 21, no. 3, pp. 2217–2220, Jun. 2011.
[18] H. M. Jang, I. Muta, T. Hoshino, T. Nakamura, S. W. Kim, M. H. Sohn, Y. K. Kwon, and K. S. Ryu, "Conceptual design of 100 HP synchronous motor with HTS field winding," in *Proc. Int. Conf. Elect. Eng. Japan*, 2002, pp. 1618–1628.
[19] Y. S. Jo, Y. K. Kwon, M. H. Sohn, K. S. Ryu, Y. K. Kim, and J. P. Hong, "High temperature superconducting synchronous motor," *IEEE Trans. Appl. Supercond.*, vol. 12, no. 1, pp. 833–836, Mar. 2002.
[20] H. M. Kim, Y. S. Yoon, Y. K. Kwon, Y. C. Kim, S. H. Lee, J. P. Hong, J. B. Song, and H. G. Lee, "Design of damper to protect the field coil of an HTS synchronous motor," *IEEE Trans. Appl. Supercond.*, vol. 19, no. 3, pp. 1683–1686, Jun. 2009.
[21] D. Wu and E. Chen, "Stator design for a 1000 kW HTSC motor with air-gap winding," *IEEE Trans. Appl. Supercond.*, vol. 21, no. 3, pp. 1093–1096, Jun. 2011.
[22] SuperPower 2G HTS wire specifications, Schenectady, NY, USA 2013. [Online]. Available: www.superpower-inc.com/system/files/SP_2G+Wire+Spec+Sheet_for+web_2013FEC_v2_0.pdf
[23] D. Hazelton and T. Lehner, *SuperPower 2G HTS wire for electrical and magnet applications* (2010). [Online]. Available: indico.cern.ch/materialDisplay.py?materialId=slides&confId=96071
[24] B. Chen, G. B. Gu, G. Q. Zhang, F. C. Song, and C. H. Zhao, "Analysis and design of cooling system in high temperature superconducting synchronous machines," *IEEE Trans. Appl. Supercond.*, vol. 17, no. 2, pp. 1557–1560, Jun. 2007.

Amir Hassannia was born in Gonabad, Iran, in February 1984. He received the B.S. degree in electrical engineering from the Ferdowsi University of Mashhad, Mashhad, Iran, in 2006 and the M.S. degree in electrical engineering in 2008 from the University of Shahrood, Shahrood, Iran, where he is currently working toward the Ph.D. degree in electrical engineering.

His research interests include design and modeling of electrical machines, superconducting motors, and fuzzy control.

Ahmad Darabi received the B.S. degree in electrical engineering from Tehran University, Tehran, Iran, in 1989, the M.S. degree in electrical engineering from the Ferdowsi University of Mashhad, Mashhad, Iran, in 1992, and the Ph.D. degree in 2002 from Queen's University, Belfast, U.K., working with the electrical machine group.

He is currently an Associate Professor with the University of Shahrood, Shahrood, Iran, where he has been with the Faculty of Electrical and Robotic Engineering since 1993. In addition, he is the Head of the Research Center for Marine Propulsions, University of Shahrood. His research activities are mostly on design, modeling, and manufacturing of miniature electrical machines and generating sets.